Development of a Spacecraft Antenna Pointing Gimbal

Charles Monroe* and Peter Rossoni*

Abstract

The development of the pointing gimbal in the high-gain antenna system (HGAS) of the Solar Dynamics Observatory spacecraft is described. The gimbal was designed for 5 years of service in Geo-Synchronous orbit. The hardware incorporates multiple levels of redundancy, allows harnessing and waveguide along its full length across its two axes of rotation and points with an accuracy of better than 0.065°. Significant issues with actuator alignment, Electrical Contact Ring noise, pointing budget, and waveguide failures are described, along with their respective resolutions.

Introduction

This paper outlines requirements, design and development activities of the SDO gimbal. Several hardware anomalies and their resolution are described. The critical reliability level was a driver for most of the issues uncovered during the gimbal development.

Significant design areas include the actuator and contact-ring mechanisms and waveguide. Unique events and lessons-learned include the encoder alignment to the actuators, noise during component-level testing, replacing flex waveguide and accommodating the harness.

Background

The Solar Dynamics Observatory (SDO), shown in Figure 1, is a NASA spacecraft that will collect data from the Sun during its 5-year life. The spacecraft was designed by and is being integrated at NASA Goddard Space Flight Center in Greenbelt, MD. Universities and industry provide its science instruments.

This observatory transfers 150Mbps (millions of bits per second) of solar imagery (with overhead) per day from its 28.5° inclination, geosynchronous orbit at 36,000 km (22,400 mile) altitude, to the ground station in White Sands, New Mexico. The gimbal geometry that is most conducive to this end is a two-axis azimuth/elevation configuration. The azimuth axis will rotate once per orbit (once per day), and the elevation axis will rotate up to ±65 degrees to allow the antenna to point to the desired Earth coordinates at the SDO Ground Station. To avoid excessive spacecraft roll maneuvers, a dual HGAS approach was taken, with antenna systems on opposite sides of the spacecraft, allowing selection of the optimum gimbal for downlink via scheduled hand-offs.

---

* NASA Goddard Space Flight Center, Greenbelt, MD

Figure 1. Solar Dynamics Observatory with One of Two High-Gain Antennas and Gimbals Circled

Driving Requirements

An important driver for the gimbal system is the downlink requirement. A rate of 150 MB/second is needed with 99.99 percent reliability over a 99 percent duty cycle.

The 99.99 percent reliability requirement reflects the transmission error rate. To achieve this percentage during periods of transmission, the azimuth axis must be able to rotate continuously without downtime for "rewinding" of the harness about the axis of rotation. This drives the need for an electrical contact ring assembly (ECRA), a slip ring or roll ring, to pass power and signal through the axis.

The 99 percent duty cycle addresses periods of fog and rain at the ground station. The spacecraft itself will occasionally occlude the view from a single antenna. A continuous downlink capability dictates two antennas—one on either side of the spacecraft. During portions of the year, a daily hand-off between antennas will be required.

These requirements lead to a highly reliable, 100% duty-cycle design, with no planned datalink interruption.

The characteristics of the antennas and the power available for transmission drive the need to keep RF throughput loss low—the gimbal itself was allocated a loss of less than 1.45 dB. To meet this requirement, an all-waveguide RF system was selected as opposed to the simpler coaxial cable approach. This necessitated waveguide rotary joints at each axis of rotation.

Also, minimizing loss drives the need for having a pointing capability of $\pm 0.30°$ to the ground station for all error sources, including spacecraft position and orientation. Of this amount, there is 0.14° budgeted for random and calibration errors of the gimbal.

Gimbal Design

The overall configuration is shown in Figure 2. The azimuth axis has unlimited rotation and the elevation axis has a $\pm$69° range. The continuous azimuth rotation is made possible by having the power and signal transferred through the ECRA. For the elevation rotation, a rotary cable wrap wherein the cable is carefully spiraled through the center of the elevation actuator manages the harness.

There are two rotating sections of waveguide on this two-axis gimbal. An azimuth section rotates with the azimuth axis and extends from the azimuth actuator up to the elevation axis. An elevation section rotates with the elevation axis and extends from the elevation actuator up to the antenna.

High Gain Antenna

Elevation Axis

Elevation RF Rotary Joint

Electrical Contact Ring Assembly (ECRA)

Azimuth RF Slip Joint

Azimuth Waveguide

Azimuth Rotary Actuator

Azimuth Axis

Azimuth RF Rotary Joint
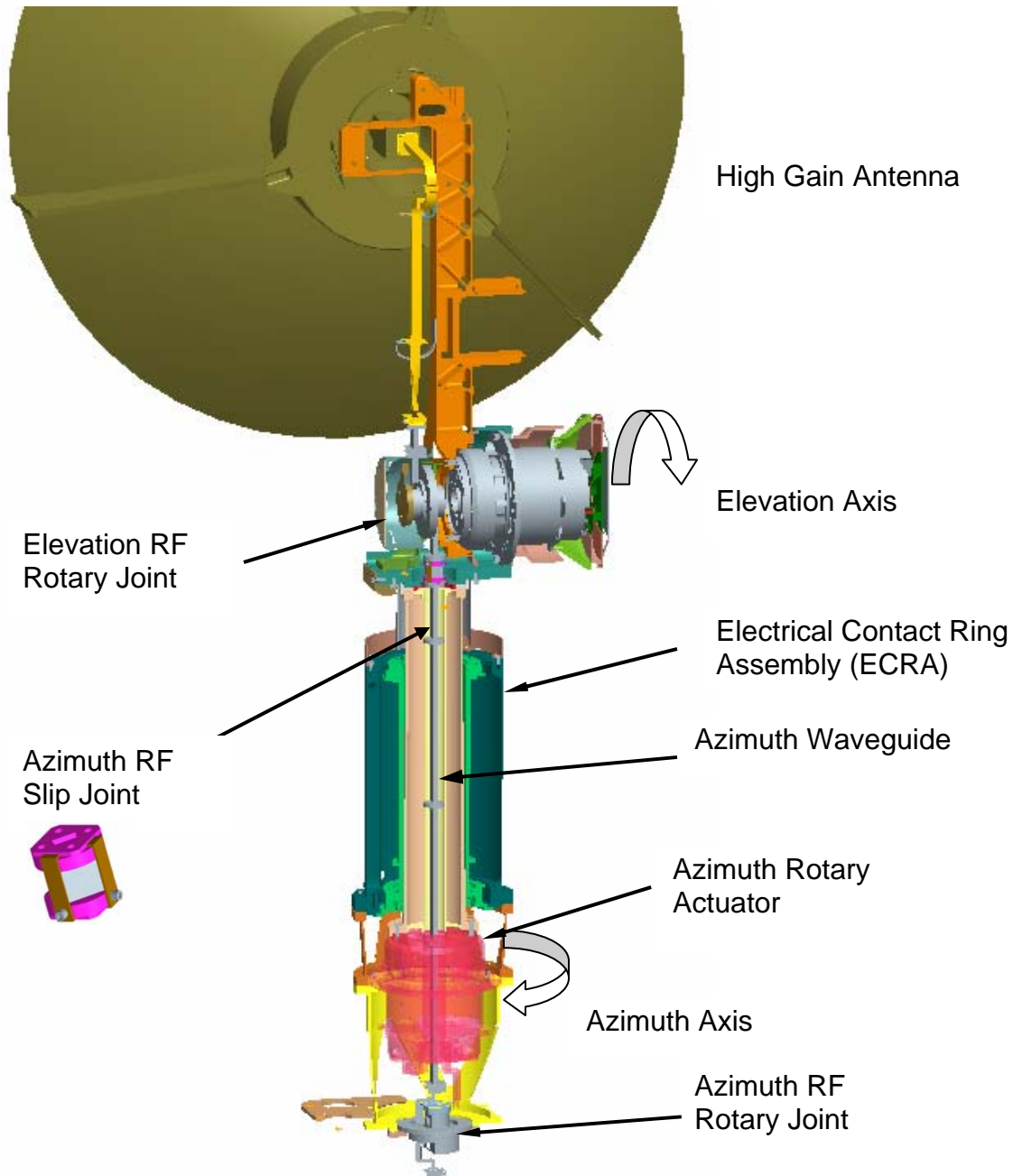
Figure 2. Gimbal Cross-section

Rotary Actuators

The rotary actuators for azimuth and elevation are identical except for hard stops on the elevation actuators limiting travel to $\pm$69 degrees. Each commercial actuator consists of a stepper motor, hybrid optical encoder, and harmonic drive gear reducer in a titanium housing. Once delivered, the units were tested for compatibility with the GSFC-designed control electronics, and characterized for settling time, torque margin, encoder output and alignment. Then thermal hardware was applied, as shown in Figure 3, and the harnessing prepared for integration to flight hardware.

Figure 3. Rotary Actuator Shown During Thermal Hardware Application

Actuator Description
The three-phase stepper motors are redundantly wound. There are two redundant encoders: a coarse encoder on the output that determines hemisphere and home, and a fine encoder on the input that counts each step taken. The actuator details are summarized below:

Actuator Parameter	Value
Output step	0.0075 degree
Harmonic drive gear ratio	200:1
Motor step	1.5 degrees
Unpowered detent torque	34 N-m (300 inch-pounds)
Max required slew speed (under the following conditions at qualification temperatures)	30 degrees/min (66.7 pulses/sec)
Driven inertia	2 kg-m^2
Driven offset load	28 N-m (250 inch-pound)
Driven friction load	2.5 N-m (22 inch-pound)

Step Settling of Bearings
On orbit, a motor step will be taken roughly every two seconds. For the actuator life test, time constraints drive the need for more frequent steps, but the period between steps should be no less than the time required for bearing balls to settle. It was decided that after the ball motion decreased to a point where the magnitude of the oscillations is less than the width of the Hertzian contact patch, the bearings would be considered essentially settled. We believe this settling criterion to be consistent with ball-pass analysis for lubricant tribo-degradation. The time required to reach this point is 35 msec, so the actuator life test could be run at ~28 pulses per sec, which is an acceleration factor of ~57.

Actuator Encoder Alignment
Actuator position is determined by internal optical encoders. Alignment of the encoder is inferred from its output. Even though settling time and torques were within requirements, some actuators had marginal

418

alignment of their encoder discs to the step detents. The easiest way to test for alignment is by the quality of the encoder output during settling in its detent. A well-aligned encoder disc would have its Light-Emitting Diode (LED) centered in the disc aperture. Even at the beginning of settle, when the oscillations are highest, little or no light would be occulted by either edge, as shown in Figure 4a (each window is two steps wide). Encoders that are not optimally aligned would shadow a portion of the light while settling in a step detent. Of 10 potential flight actuators, 6 were aligned with less than optimal performance, as shown in Figure 4b by the encoder light output "hash" during characterization testing. The actuator specification called out static alignment only; as a result, all 10 flight actuators satisfied the specification requirements.

Just prior to delivery to the spacecraft, two of the flight actuators were damaged beyond repair by excessive heat in a Goddard thermal vacuum chamber. Two of the less-than-optimal actuators were brought to flight status. These passed the static alignment specification but during a high-rate slew operation could incur positioning errors of one step. This error is reset in the control electronics when the actuator passes through the "home" position, so the condition is tolerable during slews. Under normal tracking, there is adequate time for the encoder output to settle and the output to be verified. The only remaining issue is diode output over the mission life. As the diode response decays due to radiation effects and the normal degradation due to operation, the partial occulting could reduce margin on the encoder output.
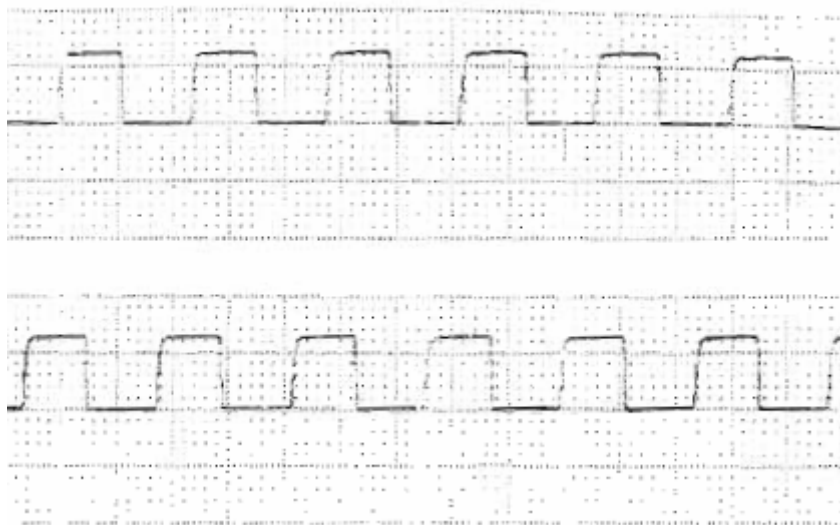
Figure 4a. Good Encoder Alignment – Two-Step Window
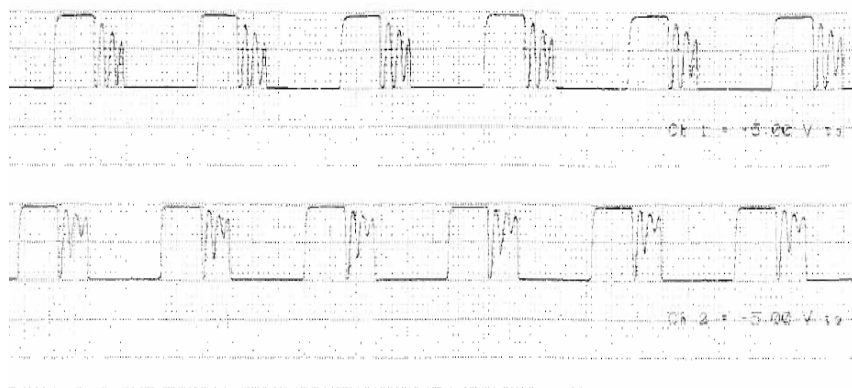
Figure 4b. Less than Optimal Encoder Alignment

Electrical Contact Ring Assembly (ECRA)

The elevation axis harness, which consists of 14 power circuits and 26 signal circuits, is routed through the ECRA. The outer structure of the ECRA, shown in Figure 5, is stationary and is hard-mounted to the same bracketry as the azimuth actuator stator. The inner structure of the ECRA is fully supported in the stationary section by a duplex set of angular contact bearings as well as a trailer bearing. A tooling ball mounted in the base of the rotating portion of the ECRA mates with a slot in the azimuth output shaft allowing the gimbal to transmit the rotary motion while permitting slight angular misalignment between the ECRA and the output shaft.

Drive
Tooling
Ball
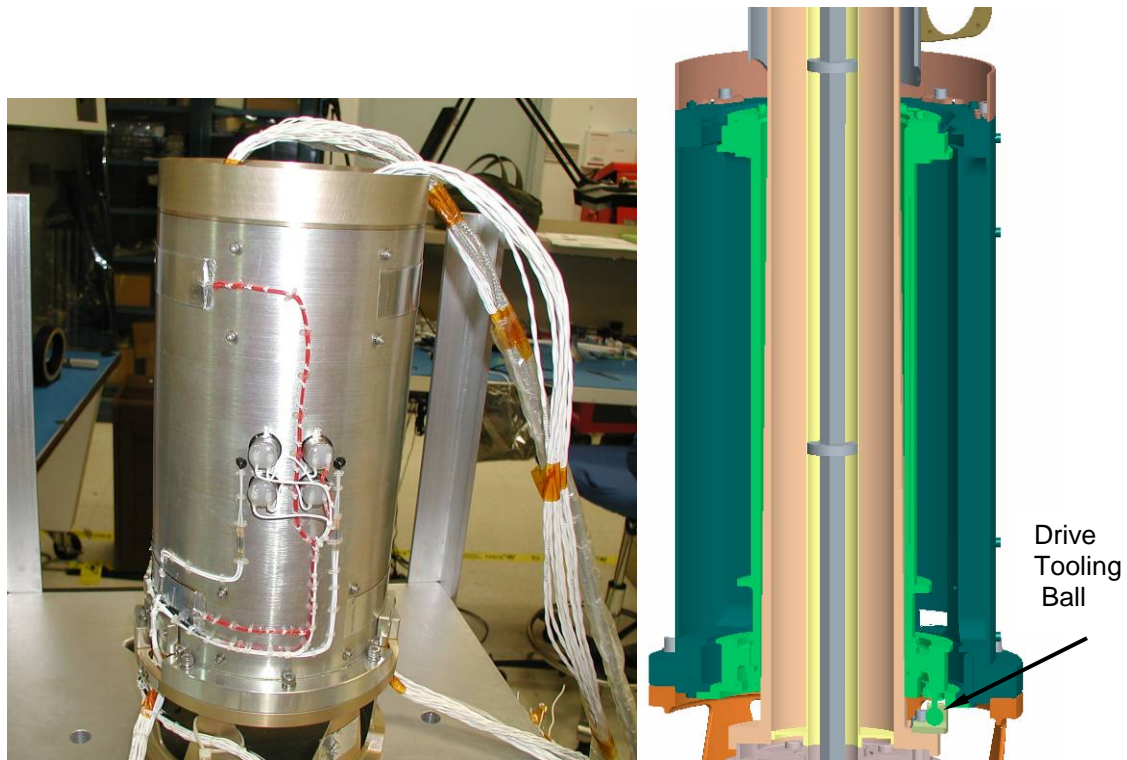
Figure 5. ECRA with Thermal Hardware Attached (prior to lead tape over wrap)

The structure consists primarily of aluminum and titanium components. The ECRA uses gold/silver/nickel alloy mono-filament brushes in gold-plated brass grooves. Two outer brush blocks that are part of the stator support brushes that span the gap between the stationary and rotary portions of the assembly. Each groove accommodates two brushes, one leading and the other trailing. The power circuits utilize a three-groove design while the lower-powered signal brushes utilize a two-groove design. The final result is a current-carrying margin in the power and signal circuits of three and four times respectively. This is in addition to the electrical redundancy in the gimbal itself.

Component-Level Test Issue
During component thermal testing, the ECRA exhibited higher than expected noise in the lines. While the ECRA exhibited acceptable noise performance at temperatures greater than 0°C, the noise levels on several circuits increased considerably at sub-zero temperatures. The primary cause was determined to be water contamination of the brush-groove lubricant. It was determined that the nitrogen environment in the thermal chamber was insufficient to purge the assembly of all water vapor. The primary solution was to perform the thermal testing in vacuum. Additional steps that were taken included a vacuum bakeout without the external housing installed before final assembly, a run-in before testing, and efforts to improve

420

the cleaning process and prevent contamination sources after cleaning. These changes to the assembly and test program resulted in power and signal circuit noise level well below the required values.

RF System

SDO's data downlink is carried out by a Ka-band RF transmission of 26.5 GHz from a ¾-meter (30 in) High-Gain Antenna to one of two 18-meter (60-ft) ground station antennas. WR-34 waveguides are used to transfer the signal from the transmitter to the HGA. They are aluminum, plated with silver. An anti-tarnish coating was applied over the silver plate. Rotary joints, shown in Figure 6, pass the RF signal with budgeted 0.2-dB insertion loss and allow rotations about the two axes. The stationary and rotating sections of each rotary joint are aligned by a duplex set of ball bearings. The rotating portion of the joint is driven similarly to the ECRA. A ball drives the movement through a slot arrangement, using a tooling ball and a clevis with a close-tolerance gap.

Drive Tooling Ball

Figure 6 RF Rotary Joint with Drive Tooling Ball (Elevation Axis Shown)

Waveguide Failure

Originally, there were two 7- to 11-cm sections of corrugated flexible beryllium copper waveguide on the gimbal—one in the azimuth section and one in the elevation section. The design intent was that the accordion-style flexibility would compensate for tolerance stack-up and for slight variations in temperature or CTE mismatches. During initial Qualification Unit vibration testing, both of the flexible sections broke completely due to low-cycle fatigue.

One cause for this failure was insufficient waveguide support. Some rigid waveguide spans were 25 cm or more, while the manufacturer recommended 15 cm or less. During vibration, it was shown by analysis that the flex waveguide saw deflections well above the yield stress point.

The main cause for failure was improper heat treatment and fabrication steps of the delicate 100-µm thick corrugated sections. Metallographic analysis of the failed waveguide revealed a larger grain size than that associated with the certified heat treatment. There are multiple conditions that can result in excessive grain size. Regardless of its cause, this condition was a primary contributor to the low cycle fatigue failure

that occurred. There was also concern with the corrugation process, which led to variable thickness. The thickness before cold forming is 125 μm. After forming, it was to be no less than 100μm. The uncertainty added to the difficulty in analyzing the part.

Other problems with the waveguide related to the braze joints between the 1mm thick rigid sections and the flex sections, a 10:1 thickness ratio. Heat from the braze operation could also have increased brittleness in the proximal region where all failures occurred. The added thickness at the joint compounded the stress concentration on the thin section.

Figure 7. Waveguide Resolution - Elevation Waveguide with "P-Trap" section

Failure Resolution
For the elevation waveguide, analysis confirmed that the 90° bend in flex could be replaced with rigid waveguide in a slightly longer, convoluted path. The addition of two more 90° bends created a shape similar to a plumbing expansion section or a P-Trap, shown in Figure 7. The extra path mitigated misalignment and thermal effects. Tolerance stack-up in the axial direction away from the P-Trap was accommodated through the use of aluminum shims.

Because of volume constraints, the azimuth section could not have bends, so two approaches were explored. The first was to procure new flexible waveguides made with properly heat-treated material, and to redesign the structural supports. New waveguides were ordered and tested with sufficient supports, and this arrangement was deemed acceptable.

The second solution, shown in Figure 2, was to replace the flexible section of waveguide with a slip-joint section. This was also developed and tested, and it was found to work well. Ultimately this slip-joint approach was determined to be more robust with no discernible failure mode, and it was selected for use in the azimuth Waveguide.

RF Path Performance
The Ka band transmission performance was tracked throughout the development process. Individual waveguide sections were scanned at various points during manufacture, test and integration. Upon delivery from the vendor the RF performance, as measured by Insertion loss and VSWR, was part of the

End-Item Data Package. Prior to integration into the gimbal, the waveguide was assembled on the bench and throughput loss measured. The budgeted and actual losses are shown in Table 1.

Table 1. Gimbal Waveguide Total Throughput Loss

	Loss (dB)
Budgeted to each Gimbal	-1.45
Highest measured in Flight Unit 1	-0.86
Highest measured in Flight Unit 2	-0.92

Pointing Capability

The characteristics of the RF system, including the transmitting and receiving antennae and the power available for transmission, drove the need for an overall allowable random pointing error of $\pm$0.30 degrees. This value includes spacecraft position knowledge, attitude knowledge and control. The gimbal portion of this pointing budget was 0.14 degree. This random error is measured on the ground to be 0.042 for the first gimbal and would have been 0.062 (not including boom-to-gimbal co-alignment) for the second.

The total budgeted error for the gimbal, including biases that can be calibrated out, is 0.87 degree. Based on ground measurements, this error is 0.175 degree for the first gimbal and would have been 0.356 for the second gimbal. The alignment budget and measurements are summarized below.

Table 2. Pointing Budget (Degrees)

	Budget				Ground Measure	
	Known on ground	Ground-to-Orbit	Random	Budget Totals	Flight 1	Flight 2
Hardware Alignment Errors						
Gimbal to boom axis co-alignment error	.13				.043	
Gimbal to HGA base I/f alignment error	.13				.162	.350
Gimbal Interaxial Orthogonality	.14	=			.007	.015
Gimbal actuator interface launch shift		.55**			.025	.018
Dynamic Pointing Errors						
Gimbal/boom dynamic interaction			.04		.011*	.011*
Gimbal tracking error			.08		.041	.061
Total on-orbit error (RSS)	.23	.55**	.09	.87	.175	.356
Total on-orbit error after compensation and on-orbit calibration (RSS)*	--	.05	.09	.14	.042	.062

* from Qualification Unit Jitter testing
** Worst case assumption
*** Ignores 0.02 degree of thermal effects allowed in budget

The launch shift was budgeted based on worst case interface assumptions, the measured value were variations measured before and after vibration testing.

For gimbal/boom dynamic interaction, the gimbal was instrumented with force gages, and the forcing function was used to derive the jitter error measurements. The item tested was an engineering test unit, flight-like in all structural respects.

For the gimbal tracking error, the budgeted amount of 0.08 degree was calculated by summing estimates for the following for each axis: harmonic drive wind-up, gear error, step latency, and wobble of the actuator output. The results were added vectorially (Root-Sum Squared). For the measured value of 0.041 degree, the rotational error and the wobble were measured for each axis and added together vectorially. Due to 1-g effects, this error is greater than the value will be on orbit.

Harnessing and Multi Layer Insulation

Some more general lessons learned deal with leaving more space for harnessing and multi-layer insulation (MLI) and addressing these details earlier in the design effort. Since the gimbal is deployed away from the spacecraft body, it is exposed to the worst radiation environment and temperature extremes on the entire spacecraft, except perhaps for the instrument complement. Protecting against this onslaught required elaborate measures that were frequently at odds with the smooth operation of a high-precision pointing mechanism.

The volumetric demands for harnessing were especially great. Even though the Tefzel®-insulated wiring is resistant to radiation, the SDO system designers implemented a policy of over-wrapping exposed actuator wires with Kapton, Lead and Aluminum tape. Because of the reliability requirements for a 5-year mission at geo-synchronous orbit, the tape layers plus the 36 wires from a single actuator formed a bundle that was approximately 15.9 mm (5/8 inch) in diameter. After wrapping, the metallic layers were each electrically bonded to ground with silver-filled epoxy.

MLI over the entire spacecraft has an electrically conductive germanium black Kapton® (GBK) outer layer. MLI is usually a challenge to bend and position in small pieces and tight quarters. The extra layers brought additional concerns as the mechanism and thermal goals conflicted. The gimbal required ten separate MLI pieces in order to protect its various convoluted surface features, as well as allow for access to the various parts. Some MLI pieces were only 15 cm (6 in) on a side. The bends and seams, such as between moving parts, are potential heat leaks that could expose the actuators to dangerous extremes of temperature. In addition, GBK is sensitive to even light abrasion such as normal hand pressure from an accidental brush against its surface. All these factors contributed to a tough challenge of constructing accurate, intricate pieces of MLI, tightly positioned, and allowing free relative motion between close-tolerance parts.

Conclusion

The first flight gimbal, shown in Figure 8, has been tested and delivered to the spacecraft. The second gimbal will be replaced by a spare after being subjected to damaging temperatures during the post-thermal vacuum bake-out. Integration and testing of the re-built gimbal is scheduled to be complete in March 2008. Launch is scheduled for late 2008.

Acknowledgements

424

Figure 8. SDO Gimbal Mated to Deploy Boom and High Gain Antenna, with MLI installed

Second Unit Shown Vertical in Background